Subtemperate regelation exhibits power-law premelting

Colin R. Meyer[1], Julia Bellamy[1,2], and Alan W. Rempel[3]

[1]Thayer School of Engineering, Dartmouth College, Hanover, NH 03755 USA
[2]Meinig School of Biomedical Engineering, Cornell University, Ithaca, NY 14853 USA
[3]Department of Earth Sciences, University of Oregon, Eugene, OR 97405 USA

July 6, 2024

Abstract

Wire regelation is a common tabletop demonstration of the pressure-dependence of the ice melting temperature where loaded wires move from top to bottom through a block of ice, yet leaves the block intact. With the background temperature fixed at the bulk melting point $\sim 0\,^\circ\mathrm{C}$, the elevated ice and liquid pressures beneath the wire cause melting because of the negative Clapeyron slope, while refreezing takes place above the wire where the pressures are reduced. Regelation is the fundamental model for temperate glacier ice moving through small bedrock obstacles. Laboratory experiments demonstrate that regelation continues to occur, albeit at much slower velocities, when the fixed background ice temperature is cold enough that the wire load is insufficient to produce bulk melting, suggesting that premelting plays a central role. Here we compile available data for wire regelation at all temperatures. We then develop a model for the subtemperate data points, where the film thickness depends on the temperature below the melting point. We find agreement between the power-law model and the laboratory data for slow regelation velocities, allowing us to characterize the dominant premelting mechanisms for different wire compositions. These results advance our understanding of the role of premelting in subtemperate glacier sliding.

1 Introduction

Regelation describes the process of an object passing through a solid by causing it to melt and refreeze. This is commonly demonstrated in a tabletop experiment where a thin weighted wire moves slowly through a block of ice, yet counterintuitively leaves the solid ice intact following the wire's passage. We show a schematic of the wire regelation tabletop experiment in figure 1. Under temperate conditions, the basic mechanisms are well-established: the elevated pressure at the wire base causes the underlying ice to melt, liberating water that flows in a narrow film and refreezes on the top of the wire where the pressure is lower; the difference in melting temperature between top and bottom enables conduction to transport latent heat. The extension of these thermomechanical

balances to describe how regelation occurs under subtemperate conditions is the focus of this paper.

Weertman (1957) first recognized the importance of regelation as a mechanism that enables glaciers to bypass small obstacles, thereby contributing to the controls on glacier sliding. Regelation remains a central component of the sliding paradigm in glaciology (cf. Cuffey and Paterson, 2010; Rempel and Meyer, 2019; Gimbert et al., 2021). Recognition that some sliding must occur under subtemperate conditions, and that this can be an important control on basal mechanics in a variety of settings (e.g. Cuffey et al., 1999; Meyer et al., 2018; Mantelli et al., 2019), motivates us to revisit this problem and examine the role of premelting during wire regelation.

Most of the literature on wire regelation has focused on cases where the ice is close to the melting point (i.e. temperate ice with $T \approx T_m = 273\,\text{K}$), due to the applicability to tabletop demonstrations performed with the surroundings at ambient room temperature. However, the focus on temperate ice is unnecessarily limiting; experiments performed under colder conditions can offer a more thorough demonstration of how ice phase behavior is affected by the pressure applied with the weighted wire. Yet, even at the melting point regelation behavior can be complicated: there is a transition from a fast regelation mode to a slow regelation regime for low applied pressures, which Drake and Shreve (1973) speculated to be affected by contaminants from the wire (cf. figure 2). Here, we seek to understand regelation experiments where the ice is held below the bulk melting temperature (i.e. subtemperate ice, $T < T_m$; e.g. Telford and Turner, 1963; Tozuka and Wakahama, 1983b; Gilpin, 1980a). Although the importance of a premelted film around the wire in subtemperate regelation experiments has been pointed out by Gilpin (1980b), Tozuka and Wakahama (1983b), Dash (1989), and Dash et al. (1995, 2006), there is more to learn. We show that we can extend the Nye (1967) analysis using the generalized Clapeyron equation and describe the full spectrum of regelation behavior.
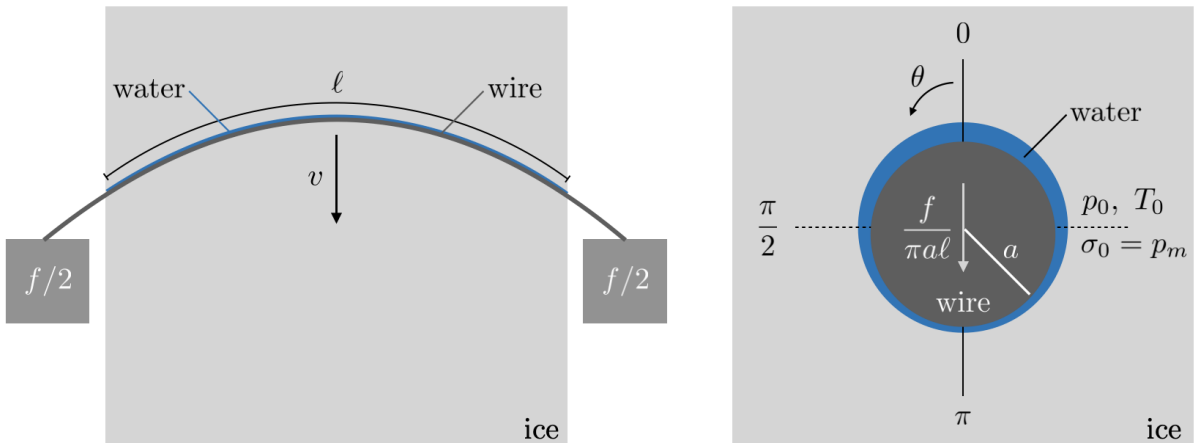

Figure 1: The wire regelation tabletop experiment: (left) a wire of length ℓ and radius a is loaded by a weight f resulting in regelation at velocity v; (right) the block of ice is at a temperature $T = T_0$, i.e. the freezer temperature, and there is a background pressure p_0. The reference pressure is p_m. Nomenclature is summarized in Table 1.

To understand the experimental landscape, we compile the published wire regelation data in figure 2. The data are scaled according to the Nye regelation velocity (equation 7 in Nye, 1967, and equation (13) below), where the effective thermal conductivity $\bar{k}$ is taken as the average between ice k_i and wire k_c conductivities, which comes out of

the heat-flow analysis in the limiting case of thin meltwater films. The gray data points are from the temperate ice experiments by Nunn and Rowell (1967), Hahne and Grigull (1972), as well as Drake and Shreve (1973), with symbols noted in the legend. Given our focus on premelting, we display the temperate points in gray to emphasize the colored subtemperate data and show that the temperate Tozuka and Wakahama (1983b) data align well with earlier experimental results. The trend is for colder experiments to produce lower regelation velocities, and there is a cluster of slow regelation data points in what we will refer to as the premelting regime.
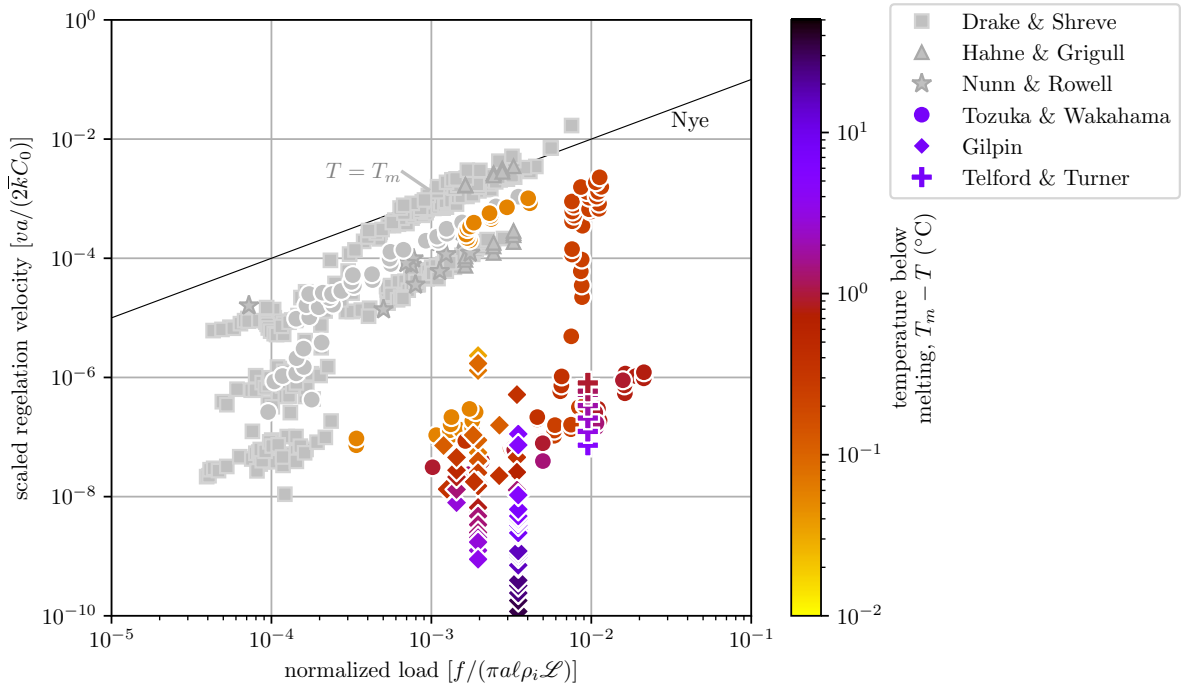

Figure 2: Collection of scaled data from wire regelation experiments with gray colors showing data at the melting point (i.e. temperate, $T = T_m$). Color datapoints show results from Tozuka and Wakahama (1983b), Gilpin (1980b), and Telford and Turner (1963) experiments where the ice block was at a temperature below the melting point (i.e. subtemperate, $T < T_m$). Nomenclature is summarized in Table 1.

Following Nye (1967), we are motivated by glacier sliding over impermeable rock and we turn to the wire regelation problem for insight because it is a simple configuration with ample experimental data; unfortunately, the subglacial environment does not have these advantages. A goal of our work is to elucidate the role of premelting in subglacial thermomechanics. For the case of a permeable subglacial system, Rempel and Meyer (2019) performed a scaling analysis of the Weertman (1957) regelation problem and re-visited the linearized Fourier analysis of Kamb (1970), using the generalized Clapeyron equation that allows for differences in ice and water pressure. Rempel and Meyer (2019) demonstrated that under well-drained conditions, facilitated by water flow through a permeable obstacle (and/or permeable ice, c.f. Fowler and Iverson, 2022, 2023), the rate of regelation can be enhanced by up to an order of magnitude in comparison with the regelation velocity anticipated under the undrained conditions that pertain when the liquid pressure is constrained to match the ice normal stress. However, their analysis does not hold in the idealized hard-bedded case involving impermeable ice separated from im-

permeable rock, wherein meltwater flow paths and the attendant hydraulic resistance are tied to thermodynamics. Indeed, the wire regelation data summarized in figure 2 suggests that regelation is likely to be inhibited in cold subglacial environments if liquid flow is restricted to thin films at the bed–ice interface (Shreve, 1984; Walder, 1986; Cuffey et al., 1999).

Here we pick up the pieces of the different existing analyses from Nye (1967), Gilpin (1980b), and Dash (1989), develop intuition, perform a scaling analysis, and describe a more complete model. In sections 2 and 2.1, we start with the generalized Clapeyron equation and force balance considerations. We demonstrate that the Nye model for regelation emerges from these ingredients alone, without any need to appeal to a full model for temperature. In section 2.2, we examine the premelting case and give a prediction for the wire speed. In section 2.3, we bolster our theory with the full temperature calculation. And, in section 2.4, we infer the premelt film thickness from the experimental data. We end with a short discussion in section 3 and some conclusions in section 4.
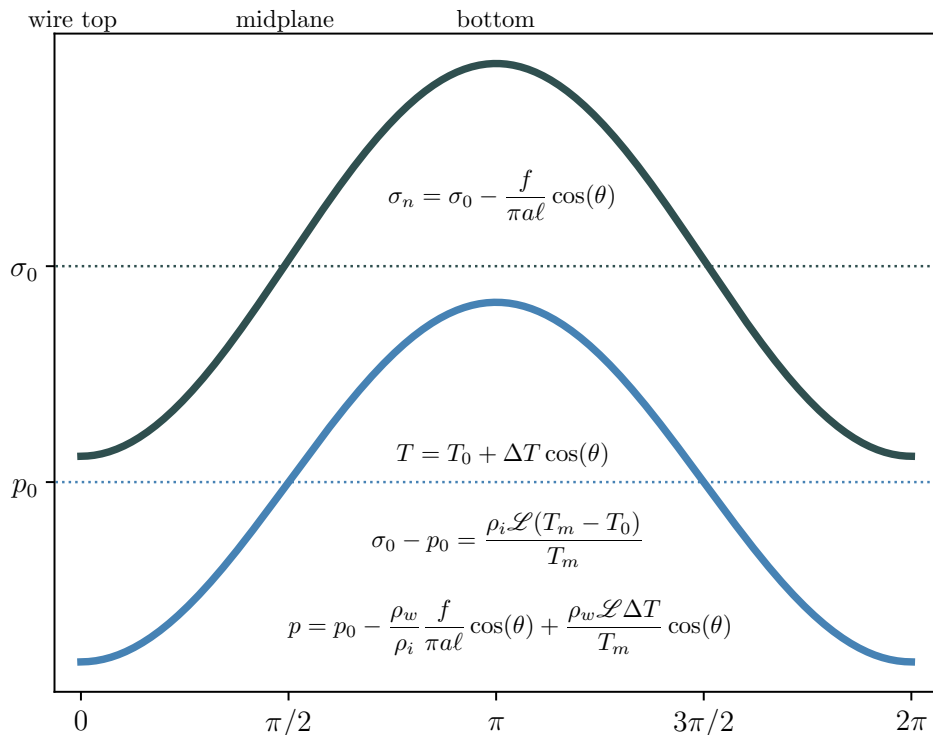

Figure 3: Schematic showing the variation of water pressure p (blue line) and ice normal stress σ_n (black line) around the wire in the premelting regime. At the midplane ($\theta = \pi/2, \ 3\pi/2$) the stress and pressure take on their background values. At the bottom (top) of the wire, the increase (decrease) in pressure and stress leads to melting (freezing). Under bulk melting (i.e. temperate) conditions, $T_0 = T_m$ and $\sigma_n = p$; premelting conditions are obtained when $T_0 < T_m$ so that $\sigma_n > p$.

2 Analysis

A weighted wire imparts a force per unit length of f/ℓ in the downwards $\theta = \pi$ direction on a horizontal, cylindrical wire of radius a that is embedded in ice, as shown in figure

1. The pressure p in the thin liquid-water film that surrounds the wire and separates it from the solid ice is a function of angular position, reaching p_0 along the midplane, where $\theta = \pi/2$. If the film is sufficiently thin that intermolecular forces can be transmitted across it between the ice and wire surfaces, then the compressive (radial) normal stress in the ice σ_n will exceed the liquid pressure p along the film–ice interface by an amount equal to the transmitted ice–wire force per unit area. Circumstances that lead to $\sigma_n > p$ define equilibrium conditions for *interfacial premelting*, whereas *bulk melting* prevails when $\sigma_n = p$. In either case, with the normal stress in the ice at $\theta = \pi/2$ defined as σ_0, geometric considerations imply that the compressive normal stress varies with angular distance as $\sigma_n = \sigma_0 - f \cos \theta/(\pi a \ell)$, as shown in figure 3.

For thermodynamic phase equilibrium, the temperature along the ice–liquid interface must vary with angular position in response to the angular changes in σ_n and p. At $\theta = \pi/2$, where the liquid pressure is p_0 and the ice normal stress is $\sigma_0 \geq p_0$, the generalized Clapeyron equation relates the equilibrium temperature T_0 (i.e. the imposed freezer temperature in an experiment) to the bulk melting temperature T_m at a reference state with the liquid pressure and ice normal stress both at p_m through (e.g. Style et al., 2023)

$$T_m - T_0 = \frac{T_m (\rho_w - \rho_i)}{\rho_i \rho_w \mathscr{L}} \left[p_0 - p_m + \frac{\rho_w}{\rho_w - \rho_i} (\sigma_0 - p_0) \right], \tag{1}$$

where ρ_w and ρ_i are the water and ice densities and $\mathscr{L}$ is the latent heat. We can choose, without loss of generality, that $p_m = \sigma_0$. The Clapeyron slope C_0 is defined as

$$C_0 = \frac{T_m (\rho_w - \rho_i)}{\rho_i \rho_w \mathscr{L}}, \tag{2}$$

which relates an increase in pressure above the reference pressure to an equilibrium temperature below the reference bulk melting point (Worster and Wettlaufer, 1999; Wettlaufer and Worster, 2006; Rempel et al., 2022; Style et al., 2023).

More generally, the variation in equilibrium temperature T as p and σ_n change around the circumference of the wire can similarly be expressed as

$$T_m - T = C_0 \left[p - p_m + \frac{\rho_w}{\rho_w - \rho_i} (\sigma_n - p) \right]. \tag{3}$$

Combining these equations and rearranging, we can express the liquid pressure that is required to satisfy the phase equilibrium constraint as

$$p = p_0 + \frac{\rho_w}{\rho_i} (\sigma_n - \sigma_0) + \frac{\rho_w \mathscr{L}}{T_m} (T - T_0). \tag{4}$$

During regelation, the applied force on the wire causes it to move at velocity v as melting occurs beneath it and the liquid flows around through the thin film to refreeze on its upper side. For lubrication flow confined to a film of thickness h with water viscosity μ, mass conservation implies that the mass of ice melted per unit time beneath angular position θ must be balanced by the water flux through the film that is driven by the liquid pressure gradient so that (e.g. Nye, 1967)

$$\rho_i v a \sin \theta = \frac{\rho_w h^3}{12 \mu a} \frac{\partial p}{\partial \theta}. \tag{5}$$

Substituting for the liquid pressure from equation (4), the regelation rate can be written as

$$v = \frac{\rho_w^2 h^3}{12\rho_i^2 \mu a^2 \sin\theta} \left(\frac{\partial \sigma_n}{\partial \theta} + \frac{\rho_i \mathscr{L}}{T_m} \frac{\partial T}{\partial \theta} \right), \tag{6}$$

with the two terms in parentheses on the right representing the contributions of normal stress and temperature variations in producing the pressure gradient that drives the compensating liquid flow.

A complete solution to the problem requires knowledge of the temperature distribution in the vicinity of the wire to properly evaluate $\partial T/\partial \theta$ around its circumference, as discussed further in section 2.3. Before examining that problem in detail, however, it is instructive to estimate the approximate sizes of the two gradient terms in equation (6) for both bulk melting and premelting cases. Regelation requires conduction at effective thermal conductivity $\overline{k}$ to remove heat from the top of the wire and supply heat to its base so that melting and refreezing can take place and facilitate wire motion. Accordingly, we anticipate that the temperature field can be expressed as $T \approx T_0 + \Delta T \cos\theta$ where the amplitude of the temperature change is expected to scale as $\Delta T \sim \rho_i \mathscr{L} va/(2\overline{k})$, assuming a roughly equal partitioning of conductive transport both through the wire and with the far-field ice. The source (sink) of ΔT is latent heat added on freezing (removed by melting). Setting $\sigma_n = \sigma_0 - f\cos\theta/(\pi a\ell)$ and substituting for the expected thermal profile into equation (6) leads to

$$v = \frac{h^3 \rho_w^2}{12\mu a^2 \rho_i^2} \left(\frac{f}{\pi a\ell} - \frac{\rho_i \mathscr{L}}{T_m} \Delta T \right) = \frac{h^3 \rho_w^2}{12\mu a^2 \rho_i^2} \left(\frac{f}{\pi a\ell} - \frac{\rho_w - \rho_i}{\rho_w} \frac{\Delta T}{C_0} \right), \tag{7}$$

where we have not made any assumptions about the relative sizes of σ_n and p in arriving at equation (7).

2.1   Bulk melting

Prior modeling efforts have focused primarily on the case of bulk equilibrium. Part of our motivation is to determine the conditions under which deviations from such a bulk equilibrium state should be expected, and to understand how the regelation velocity changes when deviations occur. To start, however, we derive the bulk equilibrium case and show that we can obtain the Nye (1967) solution as emerging from considerations of fluid flow and mass balance when phase equilibrium is enforced along the ice–liquid interface. In bulk melting, $\sigma_n = p$ along the entire circumference of the ice–liquid interface, and $\sigma_0 = p_0$. In this limit, equation (4) simplifies to

$$T - T_0 = -C_0 \left(p - p_0 \right). \tag{8}$$

Substituting the pressure field from equation (8) into the mass balance equation (5), we find

$$v = \frac{h^3 \rho_w}{12\mu a^2 \rho_i} \frac{\Delta T}{C_0}. \tag{9}$$

Hence, compatibility with equation (7) confirms the expectation gained from simple scaling considerations that under bulk melting conditions

$$\Delta T = C_0 \frac{f}{\pi a\ell}, \tag{10}$$

which states that the temperature change leading to melting and refreezing is driven by the wire load. We note that equation (10) implies that the temperature gradient term in equation (6) is only $(\rho_w - \rho_i)/\rho_w \approx 1/12^{\text{th}}$ the size of the stress gradient term. The regelation velocity is

$$v = \frac{h^3 \rho_w}{12\mu a^2 \rho_i} \frac{f}{\pi a \ell} \approx \frac{2\overline{k}C_0}{\rho_i \mathscr{L} a} \frac{f}{\pi a \ell}, \tag{11}$$

where the approximation on the right comes from setting $\Delta T \approx \rho_i \mathscr{L} v a/(2\overline{k})$ in equation (10). The effective thermal conductivity $\overline{k}$ depends on properties of the ice, the water film, and the cylindrical wire, and while reasonable *a priori* estimates can be made (e.g. assuming $h \ll a$ and a cylinder conductivity k_c close to that of ice k_i using $\overline{k} \approx (k_c + k_i)/2$), accurate determination requires a thorough analysis of the heat transport problem (see section 2.3). Based on equation (11), we can compute a scale for the film thickness h, given by

$$h \sim \left(\frac{24\mu a \overline{k} C_0}{\rho_w \mathscr{L}} \right)^{1/3}, \tag{12}$$

which ranges between $0.22\,\mu\text{m}$ and $0.46\,\mu\text{m}$ for the range of wire conductivities and the other nominal parameter values that are listed in Table 1. This is on the order of $\sim 10^3$ water molecules thick, given that water molecules are $\sim 2.75\,\text{Å}$ in size, and is sufficiently large to justify both the use of the bulk water viscosity and the neglect of intermolecular interactions between the surfaces of the ice and the wire.

We can write equation (11) nondimensionally as

$$\frac{va}{2\overline{k}C_0} = \frac{f}{\pi a \ell \rho_i \mathscr{L}}, \tag{13}$$

which is the scaling we used to plot the data in figure 2, labeled Nye. The agreement with the data shows that equation (11) can be used to calculate the regelation velocity for cases where bulk melting governs the phase behavior. Using the same scaling, equation (7) can be written nondimensionally as

$$\frac{va}{2\overline{k}C_0} = \frac{h^3 \rho_w^2 \mathscr{L}}{24\mu a \rho_i \overline{k} C_0} \left(\frac{f}{\pi a \ell \rho_i \mathscr{L}} - \frac{\Delta T}{T_m} \right), \tag{14}$$

where we treat the film thickness h as a parameter. Using the scaling that $\Delta T \sim \rho_i \mathscr{L} v a/(2\overline{k})$, we have 2 nondimensional parameters,

$$\Pi = \frac{h^3 \left(\rho_w \mathscr{L} \right)^2}{24\mu a \overline{k} T_m} \quad \text{and} \quad \delta = \frac{\rho_w - \rho_i}{\rho_w}.$$

Using these parameters equation (14) becomes

$$\frac{va}{2\overline{k}C_0} = \frac{\Pi}{\delta \left(1 + \Pi \right)} \frac{f}{\pi a \ell \rho_i \mathscr{L}}, \tag{15}$$

which implies that $\Pi = \delta/(1 - \delta)$ during bulk melting for consistency with equation (13). Given the properties listed in Table 1, $\delta \approx 0.083$ so that in this bulk melting limit $\Pi \approx 0.091$. Interestingly, the film thickness that contributes to the definition of Π is independent of the applied force, although it does depend on the wire radius and the effective thermal conductivity.

2.2 Premelting

We now return to equation (7) to examine the case where $\sigma_n \neq p$ and premelting governs the phase equilibrium. With liquid flow confined to the film that surrounds the wire circumference, mass balance implies that the regelation velocity v depends on the cube of the film thickness h, while heat flow constraints imply that v is directly proportional to the amplitude of temperature variations ΔT. Since h must shrink to become narrow enough to enable wire–ice stress transfer in cases where premelting occurs along the ice–liquid interface, we expect v to decrease substantially in comparison with bulk equilibrium cases with the same finite applied force $f > 0$; the data shown in figure 2 exhibit such velocity reductions. For consistency, to achieve slower regelation velocities in the premelting limit, heat flow considerations imply that we should also expect that the temperature amplitude ΔT must be smaller than described by the bulk melting case of equation (10). These considerations suggest that when $f > 0$ the second term in parentheses in equation (7), i.e., $\rho_i \mathscr{L} \Delta T / T_m$, must be more than $\rho_w / (\rho_w - \rho_i) = 1/\delta \approx 12$ times smaller than the first term; hence, the regelation velocity in the premelting regime should be well approximated by

$$v \approx \frac{\rho_w^2 h^3}{12 \rho_i^2 \mu a^2} \frac{f}{\pi a \ell}. \tag{16}$$

Equivalently, based on the nondimensional equation (15), we expect that $\Pi \ll \delta \ll 1$ in the premelting regime and we find that

$$\frac{va}{2\bar{k}C_0} = \frac{\Pi}{\delta} \frac{f}{\pi a \ell \rho_i \mathscr{L}}, \tag{17}$$

which is the dimensionless form of equation (16). The film thickness h is again included as a parameter in Π, and the $\Pi \ll \delta$ restriction implies that the film thickness during premelting is smaller than the film thickness during bulk melting, which is expected. Hence, the premelting regime is the slower mode of regelation in figure 2. With a film thickness of $h = 2$ nm, for example, we find that $\Pi \approx 7.6 \times 10^{-8}$, which is indeed much less than $\delta \approx 0.083$.

The intermolecular interactions that cause premelting also control the manner in which the film thickness h depends on the magnitude of $\sigma_n - p$; commonly, a power-law relationship is adopted between these two quantities (e.g. Wettlaufer et al., 1996). As before, we set the reference pressure p_m to the ice normal stress on the midplane σ_0, thereby fixing the value of T_m. Equation (1) can then be rearranged to find that $\sigma_0 - p_0 = \rho_w \mathscr{L} (T_m - T_0) / T_m$ and the film thickness for premelting cases with $T_0 < T_m$ can be expressed as

$$h \approx \lambda \left(\frac{T_m}{T_m - T_0} \right)^{1/\nu}, \tag{18}$$

where the length scale λ gauges the strength of intermolecular forces and the parameter ν signals which premelting mechanism dominates. Variations in film thickness around the wire are negligible as long as $T_m - T_0 \gg \Delta T$, which is typically expected based on the full temperature solution provided in section 2.3. Both λ and ν can be treated as constants that depend on the wire surface properties. For example, $\nu = 3$ in the idealized case where non-retarded van der Waals interactions with Hamaker constant $\mathscr{A} \equiv -6\pi \rho_w \mathscr{L} \lambda^3$ are primarily responsible for interfacial premelting and substitution of equation (18) into equation (16) predicts that for such cases the regelation velocity is inversely proportional to the temperature offset $T_m - T_0$ (Dash et al., 2006; Wettlaufer and

Worster, 2006). Other limiting values for ν include short-range electrostatic ($\nu = 3/2$), long-range electrostatic ($\nu = 2$), and retarded van der Waals ($\nu = 4$) interactions (e.g. Wilen et al., 1995; Wettlaufer et al., 1996; Rempel, 2000). In section §2.4, we use the subtemperate wire regelation data to constrain the values of λ and ν in equation (18). Despite complications, detailed calculations for ice interacting across premelted films with several well-characterized substrates (e.g. Hansen-Goos and Wettlaufer, 2010) suggest that the variation of film thickness with temperature is often well-represented by a power-law over fairly broad ranges of conditions, motivating our efforts to identify the dominant premelting behavior in the experiments by fitting for ν.

parameters	symbols	values	units
ice density	ρ_i	917	kg m^{-3}
water density	ρ_w	1000	kg m^{-3}
latent heat	$\mathscr{L}$	334,000	m^2 s^{-2}
viscosity	μ	1.8×10^{-3}	Pa · s
confined viscosity	μ_∞	3×10^4	Pa · s
bulk melting temperature	T_m	273.15	K
Clapeyron slope	C_0	7.4×10^{-8}	K Pa^{-1}
ice conductivity	k_i	2.1	W m^{-1} K^{-1}
liquid conductivity	k_ℓ	0.6	W m^{-1} K^{-1}
wire conductivity	k_c	~ 20–200	W m^{-1} K^{-1}
wire radius	a	$\sim 100 \times 10^{-6}$	m
wire contact length	ℓ	$\sim 1 \times 10^{-2}$	m
load	f	~ 1	N
freezer temperature	T_0	~ 271	K
premelting length scale	λ	$\sim 5 \times 10^{-10}$	m
power-law exponent	ν	$\sim 3/2,\ 2,\ 3,\ 4$	-
film length scale	h	$\sim 2.5 \times 10^{-9}$	m

Table 1: Table of parameters, typical order-of-magnitude of quantities, and nondimensional numbers.

2.3 Temperature field

Nye (1967) performed a detailed analysis of the temperature field surrounding a cylindrical wire that is embedded in ice that approaches its bulk melting temperature in the farfield. For clarity, we derive the temperature field from scratch. Assuming that small amounts of melting and refreezing along grain boundaries and triple junctions in the ice can be neglected, and the wire motion is sufficiently slow to ignore advective heat transport, the temperature distribution can be approximated by Laplace's equation

$$\nabla^2 T = 0, \tag{19}$$

subject to boundary conditions requiring that the temperatures and conductive heat fluxes match at the cylinder–liquid interface where $r = a$, the temperatures match at the liquid–ice interface where $r = a + h$, and the jump in heat flux across the ice–liquid interface offsets the latent heat associated with wire motion (i.e. the Stefan condition).

Together, these boundary conditions can be expressed as

$$T_c = T_\ell \quad \text{at} \quad r = a, \tag{20}$$

$$k_c \frac{\partial T}{\partial r} = k_\ell \frac{\partial T}{\partial r} \quad \text{at} \quad r = a, \tag{21}$$

$$T_\ell = T_i \quad \text{at} \quad r = a + h, \tag{22}$$

$$\rho_i \mathscr{L} v \cos(\theta) = k_i \frac{\partial T}{\partial r} - k_\ell \frac{\partial T}{\partial r} \quad \text{at} \quad r = a + h. \tag{23}$$
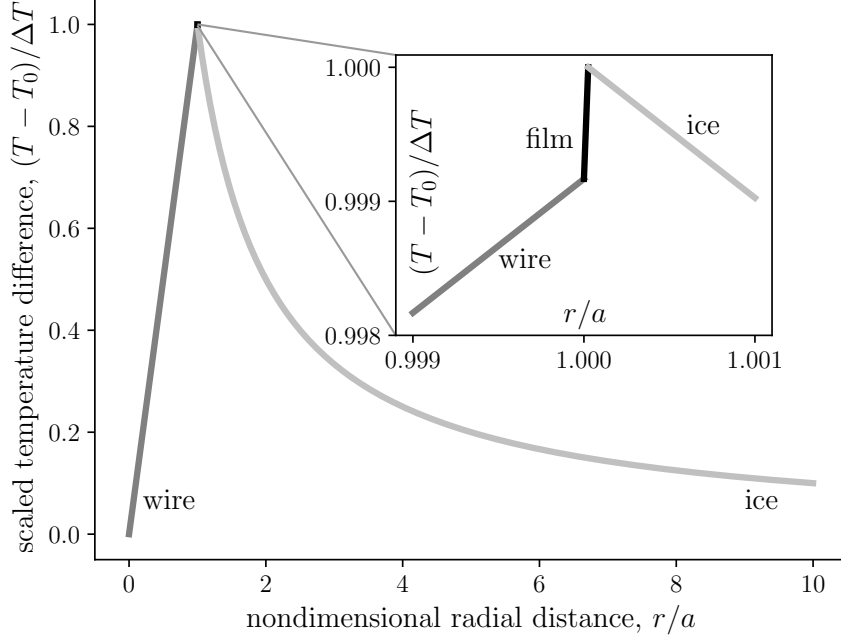

Figure 4: The scaled wire top ($\theta = 0$) temperature profile with distance from the center of the wire, following equation (24). Inset shows the modest temperature change across the narrow film.

We designate the temperature on the mid plane of the wire as T_0, i.e., the freezer temperature. Recognizing that the solutions to Laplace's equation are provided by the set of harmonic functions, the temperature field can be written as

$$T - T_0 = \begin{cases} br \cos\theta & r \le a \\ (cr + d/r) \cos\theta & a < r \le a + h \\ (e/r) \cos\theta & r > a + h \end{cases}, \tag{24}$$

where the boundary conditions are satisfied with

$$b = \rho_i \mathscr{L} v \left\{ \frac{1}{2}(k_i + k_\ell)(1 + k_c/k_\ell) + \frac{1}{2}(k_i - k_\ell)(1 - k_c/k_\ell)\frac{a^2}{(a+h)^2} \right\}^{-1}, \tag{25}$$

$$c = \frac{1}{2}(1 + k_c/k_\ell)\, b, \tag{26}$$

$$d = \frac{1}{2}(1 - k_c/k_\ell)ba^2, \tag{27}$$

$$e = \frac{1}{2}(1 + k_c/k_\ell)\, b(a + h)^2 + \frac{1}{2}(1 - k_c/k_\ell)ba^2. \tag{28}$$

10

We show the temperature solution through the top half of the wire in figure 4 for the parameters given in table 1.

On the ice–liquid interface, the temperature can be written as $T = T_0 + \Delta T \cos\theta$ where

$$\Delta T = \frac{e}{a+h} = \frac{\rho_i \mathscr{L} v \left[(1+k_c/k_\ell)(a+h)^2 + (1-k_c/k_\ell)a^2\right](a+h)}{\left[(k_i+k_\ell)(1+k_c/k_\ell)(a+h)^2 + (k_i-k_\ell)(1-k_c/k_\ell)a^2\right]}. \tag{29}$$

In the limit that $k_c h \ll k_\ell a$, as we expect for premelting around a wire, we find that

$$\Delta T = \frac{\rho_i \mathscr{L} v a}{2\bar{k}} \left[1 + \left(\frac{k_c^2 + k_\ell k_c + 2(k_i - k_\ell)k_\ell}{k_\ell(k_c + k_i)}\right)\frac{h}{a} \cdots\right], \tag{30}$$

which reduces to the scaling expression given earlier in the vanishing film-thickness limit. In figure 5, we show the scaled temperature difference $2\bar{k}\Delta T/(\rho_i \mathscr{L} v a)$ as a function the relative film thickness h/a and the ratio of the wire-to-water thermal conductivities. For relative film thicknesses that are smaller than about 10^{-1}, the first-order approximation agrees with the full solution, and for relative film thicknesses that are smaller than about 10^{-3}, we recover the scaling expression $\Delta T = \rho_i \mathscr{L} v a/(2\bar{k})$. The first-order approximation agrees well with the full expression over a broad range of variations in k_c/k_ℓ and agrees with the scaling for sufficiently thin films. Based on the values in table 1, we expect that $h/a \sim 10^{-5}$ and that the scaling expression will hold throughout; this is essentially what Nye (1967) assumed as well.
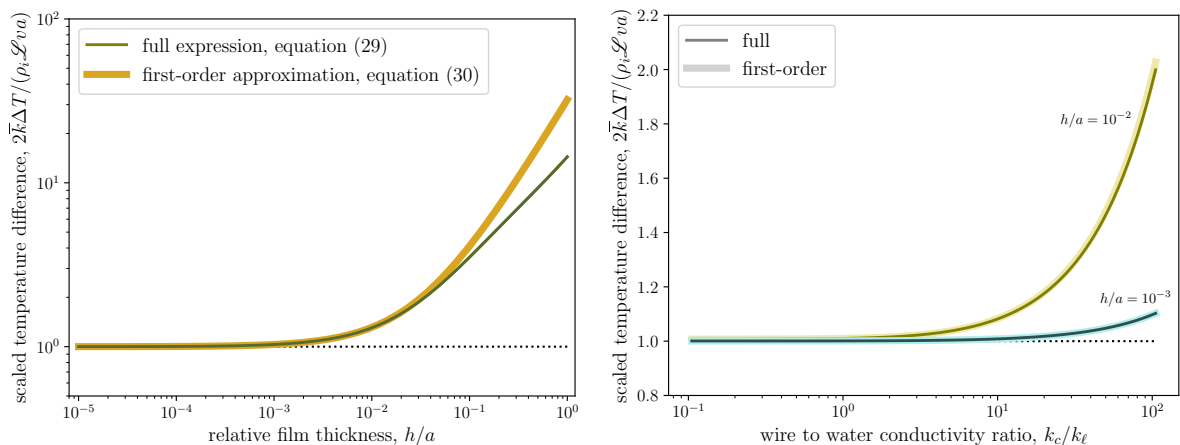

Figure 5: Scaled temperature difference ΔT as a function of (left) relative film thickness h/a and (right) ratio of wire thermal conductivity k_c to water thermal conductivity k_ℓ.

2.4 Film thickness inference

In the subtemperate and slow regelation regime equation (16) describes the wire velocity. We approximate the film thickness using equation (18), which contains two unknown parameters: an exponent ν, and a prefactor λ. We can use the data from Telford and Turner (1963), Gilpin (1980b), as well as Tozuka and Wakahama (1983b) to infer these film thickness parameters.

We start by examining subtemperate data from Gilpin (1980b) and Tozuka and Waka-hama (1983b), in which they report the regelation velocity as a function of applied load
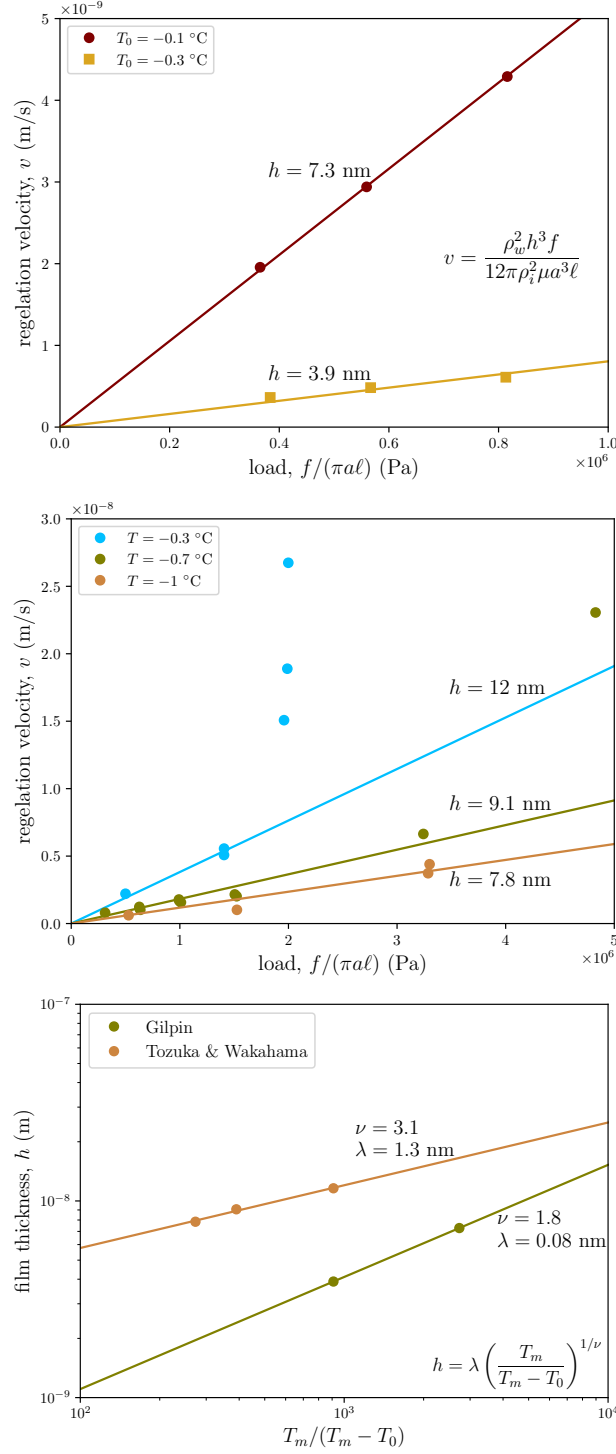
Figure 6: Slow regelation velocity with increasing load at temperatures below the melting point: (top) Gilpin (1980b) data for a wire made of the copper-nickel alloy known as constantan (inferred $h \approx 7.3$ nm and 3.5 nm at $T_0 = -0.1\,°C$ and $-0.3\,°C$, respectively). (middle) Tozuka and Wakahama (1983b) data for a steel wire (inferred $h \approx 12$ nm, 9.1 nm and 7.8 nm at $T_0 = -0.3\,°C$, $-0.7\,°C$ and $-1\,°C$, respectively). Lines show a best-fit regression that is constrained to go through the origin. We ignore the transition points and only included the slowest velocities in the regression. (bottom) inferred film thicknesses as a function of scaled undercooling, showing the premelting power-law exponent ν and prefactor λ.

at constant temperature (viz. figures 2 and 6). By finding the slope of the best-fit line between the velocity and load, we can determine the film thickness h using specified values of the viscosity μ and other properties (e.g. ρ_w, ρ_i, a) summarized in table 1. Analyzed in this way, we interpret the data for the slow regelation mode in figure 2 as resulting from variations in the film thickness with temperature. If we then fit the film thickness as a function of the scaled undercooling, we can use equation (18) to infer values for λ and ν (cf. figure 6). The results are given in table 2. For Tozuka and Wakahama (1983b), we considered only the datapoints in the slow regelation regime, before the transition, and excluded the faster data from the regression. The data suggest the premelting in Gilpin's experiments for the constantan wire is consistent with a power-law exponent midway between those derived from idealized formulations that consider short- and long-range limits of electrostatic interactions (i.e. $\nu = 3/2$ and $\nu = 2$, respectively). Tozuka and Wakahama (1983b) used a steel wire and the data suggests premelting behavior that is consistent with expectations for non-retarded van der Waals forces ($\nu = 3$). The intermolecular forces that cause premelting are sensitive to the surface properties of the wire and the ice, as well as any impurities present in the premelted liquid (e.g. Dash et al., 1995, 2006). Not surprisingly, the regelation data obtained by these two labs using different wire compositions appear to suggest that different premelting mechanisms dominate in each case. The inferred film thicknesses are nevertheless quite similar, ranging from a few nm to slightly greater than ten nm for Gilpin (1980b) as well as for Tozuka and Wakahama (1983b), based on the parameters in table 1.

dataset	$f/(\pi a \ell)$ (MPa)	T_0 (°C)	λ (nm)	ν	h (nm)	a (μm)	wire
G80	[0.3, 0.9]	-0.1	0.08	1.8	7.3	64	constantan
G80	[0.3, 0.9]	-0.3 °C	0.08	1.8	3.5	64	constantan
G80	1.07	[-35, -2] °C	0.07	1.3	[0.36, 3.6]	6.4	tungsten
G80	1.05	[-3, -0.2] °C	0.40	2.7	[2.1, 5.0]	13	tungsten
G80	0.68	[-3, -0.02] °C	0.39	2.7	[2.2, 13]	30	tungsten
G80	0.44	[-2, -0.25] °C	0.66	3.6	[1.7, 2.6]	38	chromel
T&W83	[0.3, 5]	-0.3 °C	1.3	3.1	12	150	steel
T&W83	[0.3, 5]	-0.7 °C	1.3	3.1	9.1	150	steel
T&W83	[0.3, 5]	-1 °C	1.3	3.1	7.8	150	steel
T&W83	1.7	[-3, -0.5] °C	4.6	4.3	[13, 18]	150	steel
T&W83	3.0	[-3, -0.2] °C	1.8	4.0	[5.7, 11]	150	steel
T&W83	6.5	[-0.6, -0.1] °C	0.98	3.9	[4.6, 7.5]	150	steel
T&T63	0.73	[-4, -0.5] °C	0.82	2.0	[7.5, 16]	220	steel

Table 2: Table of results for the inference of film thickness for data from Telford and Turner (1963) [T&T63], Gilpin (1980b) [G80], as well as Tozuka and Wakahama (1983b) [T&W83].

In a complementary set of experiments, Telford and Turner (1963), Gilpin (1980b), as well as Tozuka and Wakahama (1983b) measured regelation velocities as a function of temperature while keeping the load on the wire constant. In the separate panels of figure 7, we plot the inferred fluid mobility parameter h^3/μ as a function of the far-field temperature depression from bulk melting (i.e. undercooling $T_m - T_0$), and the scaled regelation velocity as a function of the scaled undercooling. The solid black line that runs through much of the mobility-parameter data highlights the expected behavior for a case with flow governed by the bulk viscosity of water and the film thickness controlled

by non-retarded van der Waals forces so that $h^3/\mu \propto 1/(T_m - T_0)$. When the under-cooling exceeds several degrees, the experimental results fall off this trend to indicate that transport becomes significantly more restricted, potentially as a result of enhanced fluid viscosity due to proximity effects when the film thickness approaches molecular dimensions. Alternatively, the decreased mobility may also be caused by a change in the dependence of film thickness on temperature, consistent with expectations if the dominant intermolecular interactions responsible for premelting changes as the film dimensions narrow. Most of Gilpin's experiments, with both tungsten and chromel wires and one set of Tozuka and Wakahama's steel-wire experiments, yielded mobility paramter values that are close to the solid trend line, the results of several other experiments are consistent with considerably higher values for h^3/μ. At the warmest temperatures, the cluster of data from Gilpin's tungsten-wire experiments that is offset to higher mobilities might be attributed to the more rapid regelation that is expected under bulk melting conditions. The two sets of experimental runs by Tozuka and Wakahama that exhibit higher mobility deviate from the solid trend line by offsets that increase with the applied load (c.f. table 2). Tozuka and Wakahama (1983b) postulate that plastic deformation of the ice may contribute towards wire motion. However, Telford and Turner (1963) report an experimental test in which they embedded a translucent (i.e. very thin) gold membrane into the ice and observed that the wire passage caused deformation that extended only a small fraction of its diameter, suggesting that plastic deformation was negligible. Nevertheless, the lone experimental set from Telford and Turner (1963) exhibits higher mobility than the trend line followed by most of Gilpin's experiments, even though it was conducted with a lower load than the single experimental set of Tozuka and Wakahama (1983b) that follows the solid trend line. A simple explanation could be that the steel wires used in these experiments had different surface properties so that the premelted films were simply thicker during the enhanced-mobility runs. It is also worth noting that the wires used by Telford and Turner (1963) and Tozuka and Wakahama (1983b) were 0.44 and 0.3 mm in diameter respectively, which is considerably larger than the wires used by Gilpin (1980b) (see table 2). If these thicker wires were comparable to the sizes of the ice crystals (not reported), it is possible that permeable flow through the tubules that line triple junctions in polycrystalline ice may have contributed to the liquid transport and resulted in the higher apparent mobilities that we inferred in figure 7.

To better illuminate how the experimental results depended on both wire composition and applied load, in the second panel of figure 7 we scale the regelation velocity following equation (16) so that the ordinate becomes h/a, i.e. the relative film thickness. For the scaled undercooling on the abscissa, we use the expression from equation (18). With logarithmic axes, figure 7 shows that the slow regelation data follow a power-law given by equation (18): each dataset falls on a line. Using regression, we can determine λ and ν simultaneously for each set of experiments and explore deviations from the overall trend depicted by the solid line in the mobility-parameter plot. The results are shown on figure 7 and given in table 2. For Gilpin (1980b) with the tungsten wire, we only consider the slow regelation data and ignore the transition to faster speeds. We find values of λ and ν that are broadly similar to those found for Gilpin's constantan wire data. For the largest load (1.07 MPa) and the lowest temperatures, we see that $\nu \approx 3/2$, which is the expected exponent for premelting dominated by short-range electrostatic interactions. For Gilpin's other two tungsten datasets, the premelting exponent is midway between those expected of long-range electrostatic and non-retarded van der Waals interactions. The film thickness increases with temperature, so that the experiments with colder tempera-
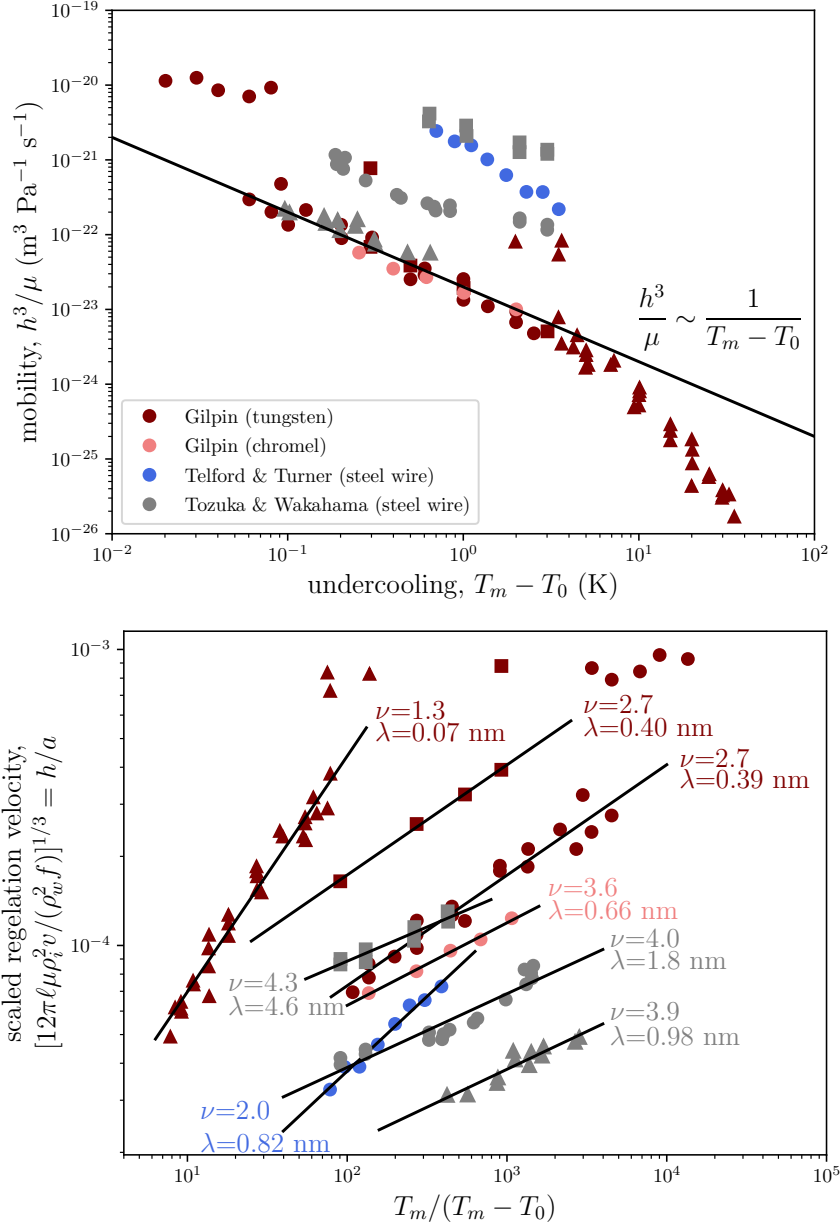
14

Figure 7: Inferred film thickness as a function of the undercooling in the slow regelation regime. The maroon (triangle: 1.07 MPa; square: 1.05 MPa; and circle: 0.68 MPa) and coral (circle: 0.44 MPa) data are from Gilpin (1980b), the blue (circle: 0.73 MPa) data are from Telford and Turner (1963), and the gray (triangle: 6.5 MPa; square: 3.0 MPa; and circle: 1.7 MPa) data are from Tozuka and Wakahama (1983b). The different datasets correspond to different wire loads, see table 2, with larger loads generally leading to faster regelation and requiring larger film thicknesses. The lines are best-fit power laws with the parameters shown on the figure.

tures have thinner premelted films than the experiments that are near the melting point. The chromel experiment reported by Gilpin (1980b) yields an exponent of $\nu \approx 3.6$, which is between the expected values for idealized cases in which non-retarded and retarded van der Waals forces dominate. The Tozuka and Wakahama (1983b) data for the steel wire yield results that are similar to those shown for the pressure variation experiments in figure 6: premelting appears to be dominated by retarded van der Waals forces. Interestingly, the Telford and Turner (1963) experiments with a steel wire suggest different values for λ and ν than the Tozuka and Wakahama (1983b) experiments with their steel wire, which could be due to differing surface properties or contaminants. The Telford and Turner (1963) data suggests premelting dominated by long-range electrostatic forces. The values of λ inferred through this data regression are in the same range as the values obtained by Wettlaufer et al. (1996) for the Wilen and Dash (1995) idealized frost heave experiment.

3   Discussion

From our analysis of published wire regelation results we obtain film thicknesses approaching microns in scale when the phase behavior around the wire is controlled by bulk melting so that the ice normal stress and film water pressure are balanced, i.e. $\sigma_n = p$, whereas film thicknesses are reduced to $\sim 1-10$ nm in the premelting regime with $\sigma_n > p$ (cf. table 2). We have attributed the dramatic reduction in regelation velocity in the premelting regime to the pronounced sensitivity of liquid flow to film thickness (i.e. $v \propto h^3$) since both the wire and the ice are treated as impermeable.

It should be noted that the inferred film thickness values reported above were obtained while using the bulk value for viscosity, although nm-scale distances represent fewer than 10 molecular diameters of water. Data from experiments on water films confined between mica sheets suggests that film thickness does not substantially affect the viscosity even down to 2 molecular thicknesses (Raviv and Klein, 2002), however, other data collected between hydrophilic substrates shows that confinement can enhance the effective viscosity by up to 7 orders of magnitude in sub-nm thick water layers (cf. Dhinojwala and Granick, 1997; Major et al., 2006). To examine the consequences, Pramanik and Wettlaufer (2017, 2019) adopted a power-law description, with $\mu_{\text{confined}} \approx \mu \left[1 + \alpha \left(h_0/h\right)^\gamma\right]$ to describe the increase in confined viscosity μ_{confined} above its normal bulk value μ as the film thickness is reduced to approach molecular dimensions h_0, at which it is enhanced by a large factor α. Reexamining data from an idealized frost-heave experiment involving premelted film flow between ice and a polyvinylidine chloride membrane by Wilen and Dash (1995), they found reasonable fits to analytical similarity solutions of their model equations by assigning $\gamma \approx 6$, $h_0 \approx 0.275$ nm, and $\alpha = 10^7$. Adopting their parameterization would lead one to expect appreciable enhancement to the water viscosity once $h \ll h_0 \alpha^{1/\gamma} \approx 4$ nm. Most of the inferred film thicknesses summarized in Table 2 exceed this level and so would be expected to be well represented using the bulk viscosity value, with the notable exception of many of the Gilpin (1980b) experimental results. Using the Pramanik and Wettlaufer (2017, 2019) confined viscosity parameterization for films that satisfy $h \ll h_0 \alpha^{1/\gamma}$ would imply modifications to the inferred premelting power-law parameters so that $\nu_{\text{confined}} \approx \nu \left(1 + \gamma/3\right)$ and $\lambda_{\text{confined}}^{1+\gamma/3} = \lambda \alpha^{1/3} h_0^{\gamma/3}$, where ν and λ are the inferred parameter values obtained using the bulk viscosity (i.e. summarized in Table 2) whereas the actual film thickness required to account for the effects of confinement would be approximated

by equation (18) using parameters ν_{confined} and $\lambda_{\text{confined}}$. Given current uncertainties in how precisely the water viscosity responds to confinement between different substrates, the inferred film thicknesses summarized here are best regarded as lower bounds. If confinement does increase the viscosity of the thinnest films, their actual thicknesses would need to be larger and the inferred power-law exponents ν reported in Table 2 would also be underestimated.

Assuming that the film viscosity does indeed match the normal viscosity of bulk water, differences between the inferred film thickness exponents ν that characterize the change in film thickness with temperature amongst the different experiments (c.f. Table 2) suggest that different mechanisms control the intermolecular forces that produce premelting. Such an inference would not be surprising given the sensitivity of intermolecular forces to poorly constrained parameters involving such factors as surface chemistry, surface charge, and impurity concentration, as well as the magnitude of the film thickness itself (e.g. Hansen-Goos and Wettlaufer, 2010). However, it is noteworthy that all three constant stress experiments using the same diameter steel wire by Tozuka and Wakahama (1983b) share similar inferred ν and two of the three experiments using different tungsten wires by Gilpin (1980b) have identical ν. The third tungsten-wire constant-stress experiment by Gilpin (1980b) extended to much colder temperatures and produced an inferred ν that was notably smaller; this difference might be partly attributed to higher film viscosities at the lowest film thicknesses and temperatures, and indeed the modest effect of reduced temperature on viscosity was not accounted for in our calculations. Moreover, results from the Tozuka and Wakahama (1983b) constant-temperature experiments suggest a lower ν than their other experiments with the same steel wire. The experiments that Telford and Turner (1963) describe used a different steel wire to obtain regelation velocities that are consistent with an even lower value for ν that was similar to that inferred from the Gilpin (1980b) constant temperature experiments with a constantan wire. Despite deviations, the experimental results show collapse onto a power-law at low temperatures, indicating a premelting regime.

It is also instructive to compare the stress and velocity of the wire regelation experiments to the same quantities in the glacier system. Driving stresses that promote the viscous flow and sliding of glaciers and ice sheets have a median value of approximately 0.06–0.07 MPa with 90% by area subjected to values less than 0.15 MPa (Meyer et al., 2018), whereas the driving stresses imposed during the wire regelation experiments examined here are considerably higher, spanning values between 0.3 and 6.5 MPa (Telford and Turner, 1963; Gilpin, 1980b; Tozuka and Wakahama, 1983a). Nevertheless, since the basal drag that resists glacier sliding can be extremely heterogeneous, local stress concentrations along the upstream surfaces of meter-scale basal obstacles can easily exceed the average driving stress by several orders of magnitude (e.g. Helanow et al., 2021) so that basal normal stresses comparable to those imposed in the wire regelation experiments are expected to be common. Reported wire regelation velocities in the premelting regime, with imposed temperatures several tenths to several degrees below bulk melting, are $\sim 10^{-2} - 1\,\text{m/yr}$. Sliding velocities beneath cold-based glaciers are difficult to constrain precisely since plastic deformation of glacial ice typically dominates surface velocity observations in these systems, but there is abundant evidence that some sliding does occur (e.g. Echelmeyer and Zhongxiang, 1987; Cuffey et al., 2000). Quantitative comparisons between the velocities observed during subtemperate wire-regelation and the velocities that characterize sliding along cold glacier beds are currently unavailable.

Warm-based glaciers often move primarily by sliding at rates that can reach up to

$\sim 10^3$ m/yr. Measured and modeled water pressures beneath glaciers commonly fluctuate on seasonal, diurnal, and even shorter time scales by up to several MPa (e.g. Andrews et al., 2014; Kavanaugh and Clarke, 2000; Rada and Schoof, 2018; Werder et al., 2013). To satisfy force-balance constraints, the normal stresses on bed obstacles must respond to compensate for these changes in the portion of the glacier weight that is supported by water pressures elsewhere. The basal permeability structure determines whether water pressures in the liquid films that separate glacier ice from bed obstacles can adjust to match the ice normal stress so that bulk melting conditions prevail, or whether imbalances can occur with $\sigma_n > p$ so that premelting takes place. The large gradients in liquid pressure that are needed under bulk melting conditions to match large gradients in ice normal stress in the vicinity of small (i.e. m-scale) bed obstacles can only be maintained if flow pathways are sufficiently restricted. Transient liquid flow driven by liquid pressure gradients and supplied by local changes in melting and freezing rates may require changes in heat flux that temporarily cool the interfacial region into the premelting regime. When this occurs, regelation rates past small obstacles may decrease dramatically, as predicted and observed for the wire regelation experiments discussed here. However, in cases where the obstacle or the ice is sufficiently permeable that the regelation rate is limited only by heat flow and liquid transport is not restrictive, no such slow-down is required. In fact, for a given change in ice normal stress across an obstacle, when the permeability is high enough that the liquid pressure is essentially uniform (i.e. $\sigma_n > p$) the difference in the equilibrium temperature predicted by equation (3) across the obstacle is much higher than in cases where the liquid pressure is constrained to match the variation in normal stress (i.e. $\sigma_n = p$); the consequent increase in conductive heat transport that occurs with $\sigma_n > p$ enables the rate of regelation to actually be higher when premelting occurs than when bulk melting prevails with $\sigma_n = p$ (Rempel and Meyer, 2019). The implication is that the distribution of basal water pressures exerts a dominant control on subtemperate regelation speeds, much as the water pressure distribution controls sliding behavior under temperate conditions as well.

4   Conclusions

Existing data for wire regelation (cf. figure 2) shows that there are two dominant regimes: a faster mode near the melting point and a slower mode for subtemperate ice. Starting from the generalized Clapeyron equation and lubrication theory, we found an expression for the regelation based on changes in stress around the wire axis and temperature variations. In this expression, we identified that bulk melting occurs when the water pressure is equivalent to the ice normal stress and derived the Nye (1967) solution using a scaling for the temperature difference based on a thin film of water, which we justify through a full temperature analysis. In the premelting limit, the water film is very thin, requiring a small temperature difference between the top and bottom of the wire and a slower regelation speed. Our general regelation expression leads to a prediction for the velocity as a function of load, where the film thickness depends on the temperature below the melting point, and we approximate this behavior as following a power law. We analyze existing regelation data to extract the film thickness under the assumption that the wire and ice are completely impermeable. Our results are consistent with previously published estimates of the premelting power-law parameters (e.g. Wettlaufer et al., 1996). We find that observed wire regelation speeds in the premelting regime are modest in comparison

with typical sliding rates beneath glaciers, yet inferred temporal and spatial variations in basal conditions suggest that premelting conditions might often prevail along portions of the ice–bed interface. Since the sizes of obstacles that significantly restrict basal motion are much larger than the typical sizes of ice grains, which themselves are often expected to be much larger than the wires used in regelation experiments, a role for porous flow that circumvents the restricted flow paths of premelted films may significantly enhance regelation rates along subtemperate glacier beds (e.g. Rempel and Meyer, 2019).

Acknowledgements

References

L. C. Andrews, G. A. Catania, M. J. Hoffman, J. D. Gulley, M. P. Lüthi, C. Ryser, R. L. Hawley, and T. A. Neumann. Direct observations of evolving subglacial drainage beneath the Greenland Ice Sheet. *Nature*, 514(7520):80–83, 2014. doi: 10.1038/nature13796.

K. M. Cuffey and W. S. B. Paterson. *The Physics of Glaciers (Fourth Edition)*. ISBN 9780123694614. Butterworth-Heinemann/Elsevier, Burlington, 2010.

K. M. Cuffey, H. Conway, B. Hallet, A. M. Gades, and C. F. Raymond. Interfacial water in polar glaciers and glacier sliding at $-17\,°C$. *Geophys. Res. Lett.*, 26(6):751–754, 1999. doi: 10.1029/1999GL900096.

K. M. Cuffey, H. Conway, A. M. Gades, B. Hallet, R. Lorrain, J. P. Severinghaus, E. J. Steig, B. Vaughn, and J. W. C. White. Entrainment at cold glacier beds. *Geology*, 28 (4):351, 2000. doi: 10.1130/0091-7613(2000)28⟨351:EACGB⟩2.0.CO;2.

J. G. Dash. Surface melting. *Contemp. Phys.*, 30(2):89–100, 1989. doi: 10.1080/00107518908225509.

J. G. Dash, H. Fu, and J. S. Wettlaufer. The premelting of ice and its environmental consequences. *Rep. Prog. Phys.*, 58(1):115, 1995. doi: 10.1088/0034-4885/58/1/003.

J. G. Dash, A. W. Rempel, and J. S. Wettlaufer. The physics of premelted ice and its geophysical consequences. *Rev. Mod. Phys.*, 78(3):695–741, 2006. doi: 10.1103/RevModPhys.78.695.

A. Dhinojwala and S. Granick. Relaxation time of confined aqueous films under shear. *J. Am. Chem. Soc.*, 119(1):241–242, 1997. doi: 10.1021/ja9632318.

L. D. Drake and R. L. Shreve. Pressure melting and regelation of ice by round wires. *Proc. R. Soc. London. Ser. A*, 332(1588):51–83, 1973. doi: 10.1098/rspa.1973.0013.

K. Echelmeyer and W. Zhongxiang. Direct observation of basal sliding and deformation of basal drift at sub-freezing temperatures. *J. Glaciol.*, 33(113):83–98, 1987. doi: 10.3189/S0022143000005396.

J. R. Fowler and N. R. Iverson. A permeameter for temperate ice: First results on permeability sensitivity to grain size. *J. Glaciol.*, 68(270):764–774, 2022. doi: 10.1017/jog.2021.136.

J. R. Fowler and N. R. Iverson. The relationship between the permeability and liquid water content of polycrystalline temperate ice. *J. Glaciol.*, page 1–9, 2023. doi: 10.1017/jog.2023.91.

R. R. Gilpin. Wire regelation at low temperatures. *J. Colloid Interface Sci.*, 77(2):435–448, 1980a. doi: 10.1016/0021-9797(80)90314-8.

R. R. Gilpin. A model for the prediction of ice lensing and frost heave in soils. *Water Resour. Res.*, 16(5):918–930, 1980b. doi: 10.1029/WR016i005p00918.

F. Gimbert, A. Gilbert, O. Gagliardini, C. Vincent, and L. Moreau. Do existing theories explain seasonal to multi-decadal changes in glacier basal sliding speed? *Geophys. Res. Lett.*, 48(15):e2021GL092858, 2021. doi: 10.1029/2021GL092858.

E. W. P. Hahne and U. Grigull. The regelation of ice—a problem of heat conduction. *Int. J. Heat Mass Transfer*, 15(5):1057–1066, 1972. doi: 10.1016/0017-9310(72)90239-6.

H. Hansen-Goos and J. S. Wettlaufer. Theory of ice premelting in porous media. *Phys. Rev. E*, 81(3):031604, 2010. doi: 10.1103/PhysRevE.81.031604.

C. Helanow, N. R. Iverson, J. B. Woodard, and L. K. Zoet. A slip law for hard-bedded glaciers derived from observed bed topography. *Sci. Adv.*, 7(20), 2021. doi: 10.1126/sciadv.abe7798.

B. Kamb. Sliding motion of glaciers: theory and observation. *Rev. Geophys.*, 8(4):673–728, 1970. doi: 10.1029/RG008i004p00673.

J. L. Kavanaugh and G. K. C. Clarke. Evidence for extreme pressure pulses in the subglacial water system. *J. Glaciol.*, 46(153):206–212, 2000. doi: 10.3189/172756500781832963.

R. C. Major, J. E. Houston, M. J. McGrath, J. I. Siepmann, and X.-Y. Zhu. Viscous water meniscus under nanoconfinement. *Phys. Rev. Lett.*, 96:177803, 2006. doi: 10.1103/PhysRevLett.96.177803.

E. Mantelli, M. Haseloff, and C. Schoof. Ice sheet flow with thermally activated sliding. part 1: the role of advection. *Proc. R. Soc. A*, 475(2230):20190410, 2019. doi: 10.1098/rspa.2019.0410.

C. R. Meyer, A. S. Downey, and A. W. Rempel. Freeze-on limits bed strength beneath sliding glaciers. *Nat. Commun.*, 9(1):3242, 2018. doi: 10.1038/s41467-018-05716-1.

K. R. Nunn and D. M. Rowell. Regelation experiments with wires. *Philos. Mag.*, 16(144):1281–1283, 1967. doi: 10.1080/14786436708229977.

J. F. Nye. Theory of regulation. *Philos. Mag.*, 16(144):1249–1266, 1967. doi: 10.1080/14786436708229974.

S. Pramanik and J. S. Wettlaufer. Confinement effects in premelting dynamics. *Phys. Rev. E*, 96:052801, 2017. doi: 10.1103/PhysRevE.96.052801.

S. Pramanik and J. S. Wettlaufer. Confinement-induced control of similarity solutions in premelting dynamics and other thin film problems. *SIAM J. Appl. Math.*, 79(3): 938–958, 2019. doi: 10.1137/18M1176300.

C. A. Rada and C. Schoof. Channelized, distributed, and disconnected: subglacial drainage under a valley glacier in the Yukon. *Cryosphere*, 12(8):2609–2636, 2018. doi: 10.5194/tc-12-2609-2018.

U. Raviv and J. Klein. Fluidity of bound hydration layers. *Science*, 297(5586):1540–1543, 2002. doi: 10.1126/science.1074481.

A. W. Rempel. *The dynamics of premelted films with geophysical applications.* PhD thesis, University of Cambridge, 2000.

A. W. Rempel and C. R. Meyer. Premelting increases the rate of regulation by an order of magnitude. *J. Glaciol.*, 65(251):518–521, 2019. doi: 10.1017/jog.2019.33.

A. W. Rempel, C. R. Meyer, and K. L. Riverman. Melting temperature changes during slip across subglacial cavities drive basal mass exchange. *J. Glaciol.*, 68(267):197–203, 2022. doi: 10.1017/jog.2021.107.

R. L. Shreve. Glacier sliding at subfreezing temperatures. *J. Glaciol.*, 30(106):341–347, 1984. doi: 10.3189/S0022143000006195.

R. W. Style, D. Gerber, A. W. Rempel, and E. R. Dufresne. The generalized Clapeyron equation and its application to confined ice growth. *J. Glaciol.*, page 1–6, 2023. doi: 10.1017/jog.2023.28.

J. W. Telford and J. S. Turner. The motion of a wire through ice. *Philos. Mag. A*, 8(87): 527–531, 1963. doi: 10.1080/14786436308211151.

S. Tozuka and G. Wakahama. Studies on regulation. 1. flow of heat in the regulation process. *J. Phys. Chem.*, 87(21):4147–4150, 1983a. doi: 10.1021/j100244a033.

S. Tozuka and G. Wakahama. Studies on regulation. 2. effect of temperature on the motion of a wire through ice. *J. Phys. Chem.*, 87(21):4151–4154, 1983b. doi: 10.1021/j100244a034.

J. S. Walder. Motion of sub-freezing ice past particles, with applications to wire regulation and frozen soils. *J. Glaciol*, 32(112):404–414, 1986. doi: 10.3189/S0022143000012119.

J. Weertman. On the sliding of glaciers. *J. Glaciol*, 3(21):33–38, 1957. doi: 10.3198/1957JoG3-21-33-38.

M. A. Werder, I. J. Hewitt, C. Schoof, and G. E. Flowers. Modeling channelized and distributed subglacial drainage in two dimensions. *J. Geophys. Res.*, 118(F20146):1–19, 2013. doi: 10.1002/jgrf.20146.

J. S. Wettlaufer and M. G. Worster. Premelting dynamics. *Annu. Rev. Fluid Mech.*, 38 (1):427–452, 2006. doi: 10.1146/annurev.fluid.37.061903.175758.

J. S. Wettlaufer, M. G. Worster, L. A. Wilen, and J. G. Dash. A theory of premelting dynamics for all power law forces. *Phys. Rev. Lett.*, 76:3602–3605, 1996. doi: 10.1103/ PhysRevLett.76.3602.

L. A. Wilen and J. G. Dash. Frost heave dynamics at a single crystal interface. *Phys. Rev. Lett.*, 74(25):5076, 1995. doi: 10.1103/PhysRevLett.74.5076.

L. A. Wilen, J. S. Wettlaufer, M. Elbaum, and M. Schick. Dispersion-force effects in interfacial premelting of ice. *Phys. Rev. B*, 52:12426–12433, 1995. doi: 10.1103/PhysRevB.52.12426.

M. G. Worster and J. S. Wettlaufer. The fluid mechanics of premelted liquid films. In W. Shyy and R. Naranyanan, editors, *Fluid Dynamics at Interfaces*, chapter 26, pages 339–351. Cambridge University Press, 1999.